Available online at www.sciencedirect.com
ScienceDirect
Journal of Nuclear Materials 360 (2007) 128–135
journal of nuclear materials
www.elsevier.com/locate/jnucmat

Defect structure of irradiated PH13-8Mo steel

W. Van Renterghem *, A. Al Mazouzi, S. Van den Berghe

SCK·CEN, Reactor Materials Research, Boeretang 200, 2400 Mol, Belgium

Received 18 May 2006; accepted 22 September 2006

Abstract

PH13-8Mo bolts, which are considered for use in the ITER reactor, were irradiated up to doses of 0.5, 1 and 2 dpa. The microstructure was investigated with transmission electron microscopy and its evolution is discussed with reference to the mechanical properties. PH13-8Mo is a precipitation hardened martensitic steel, but a large amount of austenite has been observed as well. The precipitation hardening results from the formation of small coherent NiAl precipitates in the martensite phase. Their size, size distribution and density are found to be unaffected by neutron irradiation. The dislocations in the martensite phase are mainly $a/2\langle 1\,1\,1\rangle$ type screw dislocations, whereas in the austenite phase mainly $a/2\langle 1\,1\,0\rangle$ type screw dislocations are present. The line dislocation structure did not change during irradiation, but small irradiation induced defects were observed. Using the Orowan model, it is argued that the latter are responsible for the irradiation hardening.

1. Introduction

For the design of ITER, bolts are considered for attaching the first wall panels to the blanket module [1]. The main requirements for the bolt material are high strength, satisfactory fracture toughness, and good resistance against fatigue and neutron irradiation [2]. More specifically, the stress relaxation under irradiation is a key factor, as the bolts must retain their stress to keep the panels in place.

One of the candidate alloys is PH13-8Mo, a precipitation hardened martensitic steel. The general thermal cycle for this steel consists of a normalization process and an ageing process. After the normalization process, the alloy is transformed completely to the martensite phase [3], although in the weld of this alloy [4] or after fast quenching [5], some austenite is still observed.

Ageing the solution-treated material for 4 h at temperatures above 500 °C induces hardening which is the result of the precipitation of the ordered NiAl phase [3,5,6]. This phase has a B2 (CsCl) crystal structure with a lattice parameter of 0.2882 nm. The lattice mismatch with the martensite structure is very small and hence, large coherent particles can be formed which make the steel highly resistant to overageing [3]. A side effect of this treatment is the reversion of some martensite to austenite which remains after the subsequent cooling to room temperature [3].

The mechanical properties of this material, before and after irradiation have been described

* Corresponding author. Tel.: +32 14 33 30 98; fax: +32 14 32 12 16.
E-mail address: wvrenter@sckcen.be (W. Van Renterghem).

0022-3115/$ - see front matter © 2006 Elsevier B.V. All rights reserved.
doi:10.1016/j.jnucmat.2006.09.009

by Hooijmans et al. [7] and Schmalz et al. [8]. As a result of the precipitation hardening, a high yield strength of 1331 MPa at 20 °C and 1129 MPa at 300 °C is measured before irradiation. The evolution of the yield strength under tensile conditions as a function of dose demonstrates that this material hardens under irradiation up to 1525 MPa at 20 °C and 1300 MPa at 300 °C after a dose of 2.5 dpa. The irradiation-induced stress relaxation is limited and a relatively high fraction of 60% of the initially applied stress is retained after irradiation to 2.5 dpa.

For better understanding of the mechanical properties under irradiation, an investigation of the defect structure of irradiated PH13-8Mo bolts was performed. Transmission electron microscopy (TEM) was applied to determine the defect structure and its evolution versus dose. The objective of this investigation is to relate the changes in microstructure to the changes in mechanical properties.

2. Experimental procedures

The composition of the investigated PH13-8Mo steel is given in Table 1. The material was received in the form of bolts with a shaft of 1.5 mm, in the solution-annealed and quenched conditions. Precipitation hardening was performed at NRG-Petten [7]. The steel was solution treated at 930 °C for 1 h, cooled in furnace to 150 °C and further cooled in air to a temperature below 15 °C. The material was kept at that temperature for at least 2 h. Subsequently, the material is precipitation-hardened at 560 °C for 4 h.

The specimens were irradiated at NRG-Petten in the STROBO-03/04/05 irradiation experiments in the high-flux reactor [9]. The average neutron flux ($E > 1.0$ MeV) was calculated to be 0.689×10^{14} n cm^{-2} s^{-1} and the irradiation was performed at a temperature of 300 °C. The bolts were irradiated for 75, 125 and 250 full power days giving doses of around 0.5, 1 and 2 dpa, respectively.

The radioactivity of one bolt is of the order of 10^{10} Bq. Therefore, most steps of the specimen preparation had to be performed in a hot cell. Slices were cut from the shaft of the bolt and mechanically polished to a thickness of about 100 μm. Reducing the size of the specimen also reduces its activity and after the mechanical polishing, the activity was sufficiently low to take the specimens out of the hot cell and to treat them in a fume hood. The specimen was glued on a golden grid of 3 mm with a hole of 1 mm using M-bond 610 adhesive. The final step in the specimen preparation was electrochemical polishing. The electrolyte consisted of 5% perchloric acid and 95% methanol. The temperature was −50 °C and the applied voltage was 40 V.

The specimens were investigated in a JEOL 3010 TEM operating at an accelerating voltage of 300 kV. Conventional bright field, dark field, weak beam imaging and electron diffraction techniques were used. The local thickness of the specimen was determined using convergent beam electron diffraction (CBED) patterns under two beam conditions [10].

3. Results

3.1. Grain structure

The bright field TEM-image in Fig. 1(a), shows the lath-like grain structure which is typical for the martensite phase in low carbon steels [11]. From XRD measurements, it has been reported that the martensite in PH13-8Mo has a bcc lattice [3]. The diffraction patterns obtained during this TEM investigation, however, proved that both the bcc martensite and fcc austenite were formed. For example, in the diffraction pattern in Fig. 1(c) the (002) reflections of both the austenite and the martensite phase are present. A small angle of 9° was measured between the two (002) type reflections. This angle is in agreement with the Kurdjumov–Sachs orientation relation between the austenite phase and the martensite phase [11]. It was observed in dark field images that all martensitic bcc laths have the same orientation and also the austenitic fcc grains have the same orientation.

Only a few examples are shown in Fig. 1, but similar images were obtained in the unirradiated specimen as well as in all irradiated specimens. It was

Table 1
Chemical composition (wt%) of PH13-8Mo

	C	Mn	Si	P	S	Cr	Mo	Ni	Al	Fe
PH13-8Mo	<0.027	0.06	0.02	0.005	0.001	12.72	2.19	8.20	1.07	75.71

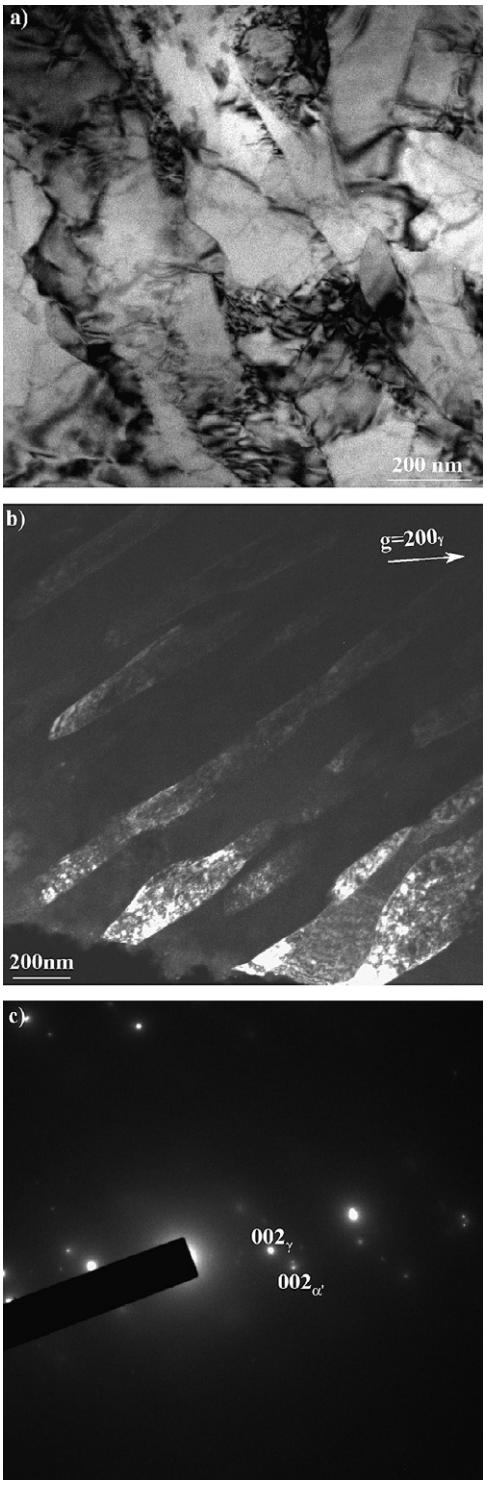

Fig. 1. (a) Bright field image of the grain structure of PH13-8Mo and (b) dark field image of the grain structure in the 0.5 dpa specimen using the (200) reflection of the austenite phase. (c) The corresponding diffraction pattern showing the orientation relation between the martensite (α') and the austenite phase (γ).

attempted to quantify the volume fraction, but using TEM images, the results are inaccurate because only the projected structure of a limited area can be visualized. The TEM images show no obvious differences in the volume fraction of each phase upon irradiation.

3.2. Precipitates

Because of the bcc crystal lattice of the martensite phase, planes with Miller indices of which the sum is uneven, for example {100} or {111} planes, do not generate reflections in the diffraction patterns. As shown in Fig. 2(a), however, some intensity was observed at those positions. When a dark field image is recorded using these reflections, images as in Fig. 2(b) are obtained which show the presence of a large number of spherical particles forming small coherent precipitates. Because of their coherence they are not visible in bright field images or dark field images using a martensite matrix reflection, as in Fig. 2(c).

The formation of NiAl enriched precipitates in PH13-8Mo steel has been reported in literature [3,5,6]. They are found to be coherent with the martensite and have a B2 (CsCl) crystal structure with a lattice parameter close to that of the martensite phase. In the diffraction pattern, reflections are generated at the same location as the martensite, but because the scattering factors of Ni and Al are sufficiently different, no diffraction reflections are forbidden and also the {100} and {111} reflections are visible in the diffraction pattern.

The size and density of the precipitates were measured from dark field images recorded using a superstructure reflection like in Fig. 2(b). Under those conditions, only the precipitates are bright, allowing the measurement of their density and size. The average size was (7.0 ± 0.5) nm and the density $(1.9 \pm 0.4) \times 10^{22}\ \mathrm{m}^{-3}$.

No NiAl precipitates were found in the austenitic phase, but occasionally, $M_{23}C_6$ carbides were observed. Contrary to the NiAl precipitates, the carbides have a coarse shape and are much larger. They are formed close to the grain boundaries between an austenitic and a martensitic lath.

The precipitates which were found in the martensitic phase of the unirradiated material are still present in the irradiated specimens. Examples for each dose and the corresponding diffraction patterns are shown in Fig. 3. In the diffraction patterns, superstructure reflections generated in coherent NiAl precipitates

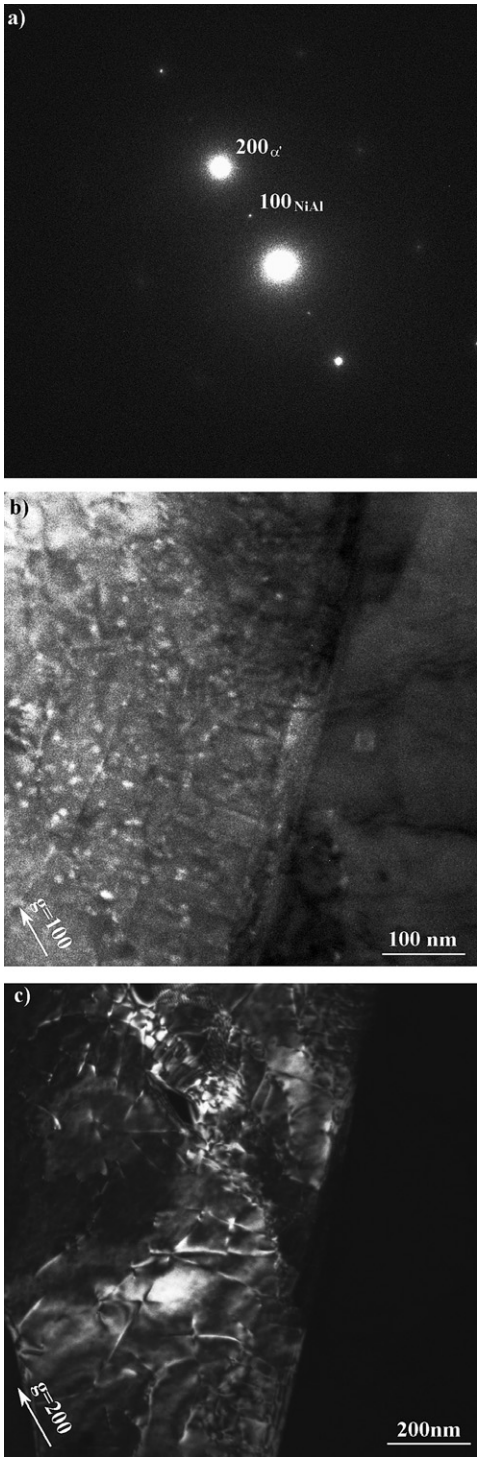

Fig. 2. (a) Diffraction pattern showing the (200) reflection of the martensitic phase of PH13-8Mo steel (α') and a superstructure reflection (NiAl) on the (100) position. (b) Dark field image using the (100) superstructure reflection, showing the size and density of the precipitates and (c) dark field image of the same region using the (200) matrix reflection of (a). The coherent precipitates are not visible under these conditions.

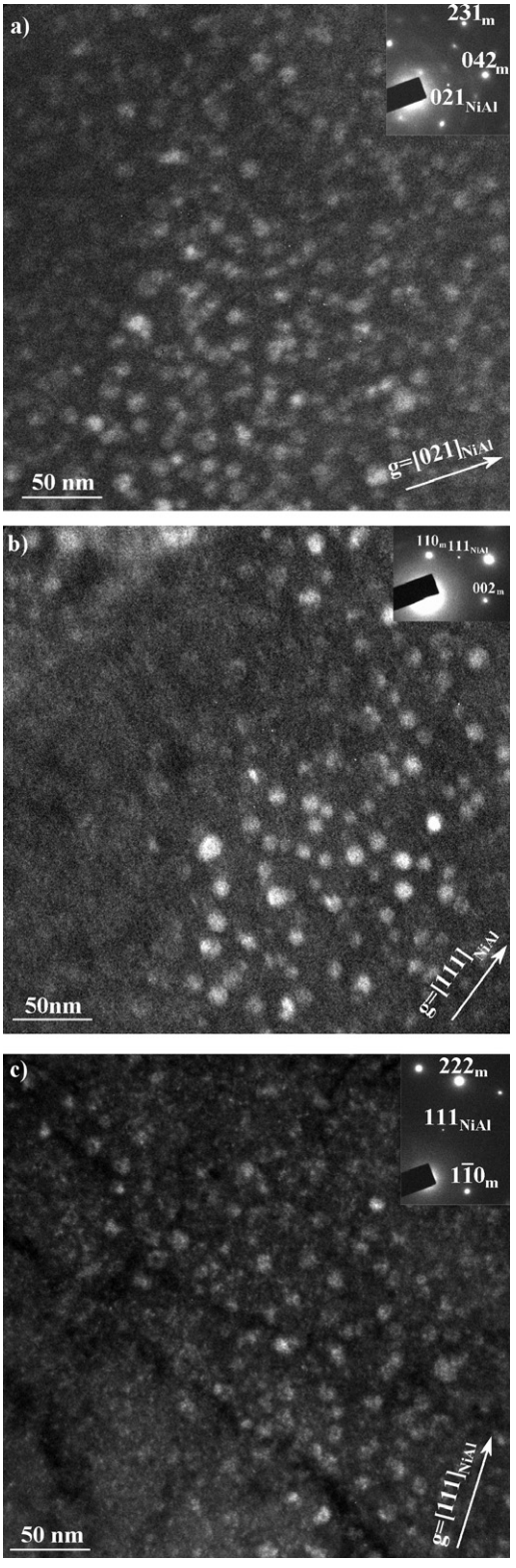

Fig. 3. Dark field images showing the precipitates in the specimens irradiated to (a) 0.5 dpa, (b) 1 dpa and (c) 2 dpa.

Table 2
Average size and density of NiAl precipitates in the martensitic phase of PH13-8Mo steel

Specimen (dpa)	Average size (nm)	Density (10^{22} m^{-3})
0	7.4 ± 0.5	1.9
0.5	7.7 ± 0.5	2.0
1	7.4 ± 0.5	1.8
2	7.4 ± 0.5	2.6

are still present. This means that no amorphization of the precipitates has occurred, as could be expected at this high irradiation temperature [12].

The precipitate density, size and size distribution of the three irradiated specimens were determined and the results are reported in Table 2. For all specimens the average size equals about (7.4 ± 0.5) nm. The precipitate density fluctuates around 2.0×10^{22} m^{-3}. Also the size distributions are comparable. The average sizes, size distributions and densities show that no precipitates are removed and that they did not grow or shrink. Consequently, these results show that the irradiations at 300 °C have not affected the precipitates formed in the martensitic phase of PH13-8Mo steel.

3.3. Dislocations

In both the martensite and the austenite grains, a considerable amount of dislocations is found. The measured dislocation density equals $(4 \pm 1) \times 10^{14}$ m^{-2} for both phases. The high dislocation density is most probably due to the presence of the two phases with a different crystal structure which introduces stress in the material. In general, a high amount of dislocations is formed in the martensite laths [11].

The type of dislocation was determined from extinction conditions in comparison with the expected dislocation types. The martensite phase has a body-centered cubic structure and in these types of crystals, dislocations with an $a/2\langle 1\,1\,1\rangle$ Burgers vector are preferentially formed [13]. The austenite phase has a face-centered cubic structure and dislocations having an $a/2\langle 1\,1\,0\rangle$ Burgers vector are expected [13].

The dark field images in Fig. 4 confirm that the expected dislocation types are formed. The three images were recorded from the same area, but using different diffraction vectors. For Fig. 4(a) and (b), the specimen was oriented close to the [1 1 1] zone and the $(\bar{2}\,1\,1)$ and $(0\,1\,\bar{1})$ diffraction vectors were used respectively. For Fig. 4(c), the specimen was

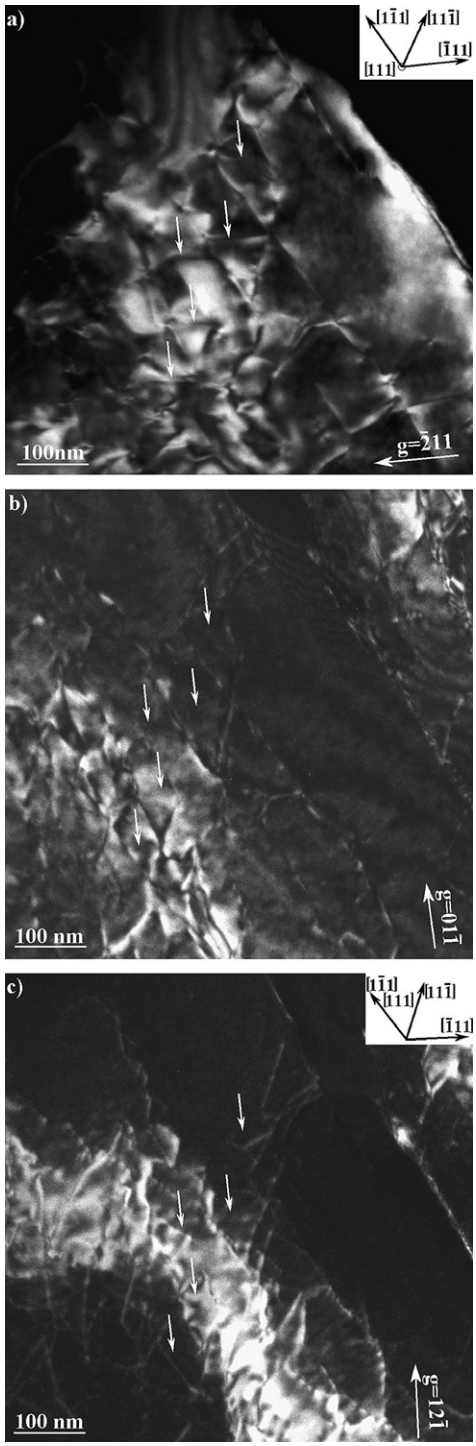

Fig. 4. Determination of the Burgers vector of the dislocations by three dark field images. In (a) and (b) the specimen is oriented close to the [1 1 1] zone, while in (c) it is oriented close the [1 0 1] zone. The diffraction vectors used are indicated. The white arrows point towards 5 of the dislocations which are extinct in (b) and (c). The insets in (a) and (c) show the projections of the four $\langle 1\,1\,1\rangle$ directions on the image plane.

oriented close to the [1 0 1] zone and the diffraction vector was $(1\,2\,\bar{1})$. The dislocations indicated by the white arrows in Fig. 4(a) are extinct in Figs. 4(b) and (c). Applying the $\mathbf{g}\cdot\mathbf{b} = 0$ extinction criterion, the Burgers vector was calculated to be $a/2[\bar{1}\,1\,1]$. In Figs. 4(a) and (c) the projections of the different $\langle 1\,1\,1\rangle$ directions on the image planes are indicated. Most dislocation contrast lines are parallel to these projections and the dislocations with the $a/2[\bar{1}\,1\,1]$ Burgers vector are parallel to the projections of the $[\bar{1}\,1\,1]$ direction. It was calculated that only the $[\bar{1}\,1\,1]$ direction corresponds with these two projections. Because the Burgers vector is parallel to the direction of the dislocation, these dislocations are screw dislocations. Not all dislocations in the martensite phase were analyzed in such detail, but all of the observed extinction conditions and the majority of the dislocation directions are in agreement with $a/2\langle 1\,1\,1\rangle$ type screw dislocations.

A similar analysis was performed in the austenite phase, but to avoid overloading the paper, it will not be discussed in detail. It was found that the observed extinction conditions and dislocation lines correspond in most cases with $a/2\langle 1\,1\,0\rangle$ type screw dislocations.

The type of dislocation and their density were also investigated in the irradiated PH13-8Mo specimens. Similar results as for the unirradiated specimen were obtained. This means that, in the martensitic phase, $a/2\langle 1\,1\,1\rangle$ type screw dislocations were found, while in the austenitic phase $a/2\langle 1\,1\,0\rangle$ type screw dislocations are formed. The dislocation structure has not changed with irradiation.

3.4. Radiation damage

The major effect of the radiation on the microstructure of PH13-8Mo steel is the formation of vacancies and interstitials which agglomerate and form dislocation loops. These are the defects usually introduced by irradiating a steel specimen [14]. The contrast introduced by small dislocation loops can be very similar to the contrast of small precipitates and care has to be taken to distinguish between both defects. In these samples, the coherency of the precipitates can be exploited to this purpose. As mentioned in Section 3.2, the precipitates are not visible when using a matrix reflection for the dark field image. Therefore, under those conditions, only the irradiation-induced defects are visible.

Typical images are shown in Fig. 5. A dark field image of the specimen before irradiation is shown in

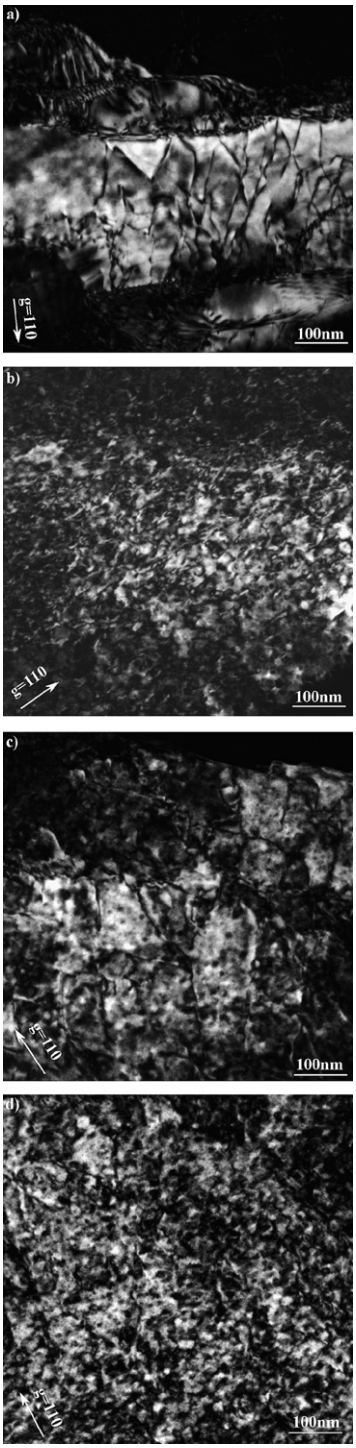

Fig. 5. (a) A typical dark field image of the specimen before irradiation, showing that under these conditions the precipitates do not contribute to the contrast. (b)–(d) Radiation damage in PH13-8Mo steel with a dose of (b) 0.5 dpa, (c) 1 dpa and (d) 2 dpa. The damage can be recognized by the round dark contrast formed by small dislocation loops, which is not present in the unirradiated specimen.

Table 3
Density and average size of the radiation induced defects

Dose (dpa)	Defect density (10^{22} m^{-3})	Average size (nm)
0.5	0.4	3.8
1	1.6	5.6
2	2.8	6.2

Fig. 5(a). Several dislocations can be seen, but the background intensity is smooth. The dark field images of the irradiated specimens of Fig. 5(b)–(d), recorded under similar conditions, show a different structure. The background is no longer smooth, but a large amount of small defects determine the contrast. This contrast is not introduced by the precipitates, although they are present in the same area. In that case, a similar kind of contrast should be visible in the specimen before irradiation, when a dark field image is recorded using a matrix reflection, but no such contrast can be observed in Fig. 5(a). Most probably this contrast is introduced by small dislocation loops.

The density and size of the radiation induced defects were measured. Similar results were obtained in the austenite and the martensite phase, and a single value for the entire specimen is given in Table 3. With increasing dose, the loop size increase from 3.8 nm to 6.2 nm and the density increase from 0.4×10^{22} m^{-3} to 2.8×10^{22} m^{-3} were determined. In the discussion, it will be argued that this observation is in agreement with the irradiation hardening reported by Schmalz et al. [8].

4. Discussion

The tensile tests performed on the PH13-8Mo specimens show that the hardness increases with increasing dose [8]. It was observed in the microstructure analysis that the grain structure, the dislocation structure and the precipitates are not significantly affected by the radiation. Therefore, the hardening can only be explained by the formation of small defects, like dislocation loops, which were observed in the irradiated specimens.

Irradiation hardening as a result of small vacancy or interstitial dislocation loops is a well known phenomenon in steels. The hardening is explained by the Orowan mechanism, which states that the small dislocation loops act as dispersed barriers for dislocation glide. The increase in yield stress ($\Delta\sigma$) as a result of these barriers depends on the number of defects and their size and can be calculated [15] as:

$$\Delta\sigma = \alpha M \mu b (Nd)^{1/2},$$

where M is the Taylor factor, α is a dimensional constant related to the strength of the barrier, μ is the shear modulus, b the Burgers vector of the moving dislocation and $Nd^{1/2}$ is the mean discrete obstacle spacing with N being the number density of the obstacles and d their diameter.

The measured stress increase is compared to the calculated increase using the formula given above. The values for the parameters are M=3.06 [16], $\mu = 80.6$ GPa [3], and $b = 0.254$ nm, the average length of the Burgers vector of the dislocations observed in the austenite and martensite phase. The measurements for N and d are given in Table 3. The value of α is not known, but the graph in Fig. 6 demonstrates that reasonable agreement between the experimental and the calculated values can be obtained if a value of 0.15 is assumed for α. For comparison, also the graphs for $\alpha = 0.1$ and 0.2 are shown in Fig. 6.

No reference data were found in literature for PH13-8Mo, but some values for α in F82H, a ferritic/martensitic steel, were found [15,17]. For F82H, the irradiation-induced dislocation loops are considered as weak obstacles and the α value equals 0.1. Comparison of the experimentally measured hardening and the hardening calculated based on the Orowan mechanism, yielded $\alpha = 0.3$. The difference between these values was explained by suggesting a contribution of other defects, like voids or helium bubbles, to the hardening.

In view of the results for F82H, it can be concluded that the value of $\alpha = 0.15$ is not unreasonable for the strength of the dislocation loops and

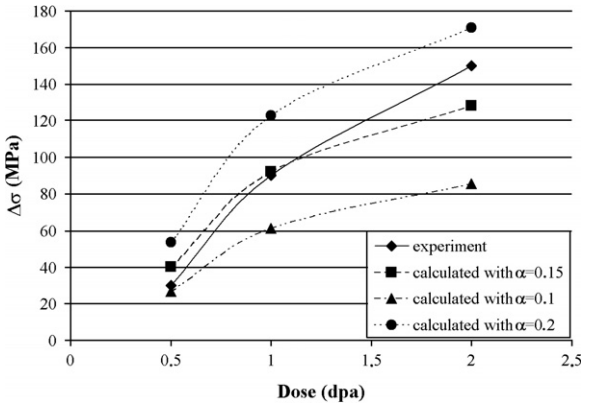

Fig. 6. Comparison of the calculated increase in yield stress with different values for the dislocation loop strength to the experimentally measured values.

that, for this alloy, the measured increase in hardness can be explained by the formation of small dislocation loops.

5. Conclusions

The evolution of the defect structure of PH13-8Mo bolts irradiated to doses of 0.5, 1 and 2 dpa, was evaluated using transmission electron microscopy and related to the changes in mechanical properties.

It was demonstrated that both the martensite and austenite phases are present in the provided specimens. There is a Kurdjumov–Sachs orientation relation between the two phases. NiAl precipitates were found in the martensite phase, but not in the austenite phase. The precipitate density, the average size and size distributions do not change after irradiation, which shows that the precipitates are not affected by the radiation. No changes in the dislocation structure were observed. In the martensite phase mainly $a/2\langle 1\,1\,1\rangle$ type screw dislocations are formed, whereas in the austenite phase the dislocations were characterized to be $a/2\langle 1\,1\,0\rangle$ type screw dislocations.

Small irradiation-induced defects were observed. Their density and size increase with increasing dose. These defects are responsible for the irradiation hardening measured in the mechanical tests. The increase in strength was calculated based on the Orowan mechanism of hardening. A good agreement between the calculations and measurements was obtained when a value of $\alpha = 0.15$ is assumed. The irradiation-induced increase in hardness can be fully explained by the formation of the small dislocation loops.

Acknowledgements

This work has been partially funded by the European Fusion Programme under EFDA task TW1-TVV-BOLMAT. The authors would like to acknowledge F. Swinnen for the specimen preparation in the hot cell.

References

[1] F. Elio, K. Ioki, P. Barabaschi, L. Bruno, A. Cardella, M. Hechler, T. Kodama, A. Lodato, D. Loesser, D. Lousteau, N. Miki, K. Mohri, R. Parker, R. Raffray, D. Williamson, M. Yamada, W. Daenner, R. Mattas, Y. Strebkov, H. Takatsu, Fusion Eng. Design 46 (1999) 159.
[2] R. Scholz, R. Matera, Fusion Eng. Design 51&52 (2000) 165.
[3] V. Seetharaman, M. Sundararaman, R. Krishnan, Mat. Sci. Eng. 47 (1981) 1.
[4] W.T. Delong, G. Ostram, E. Szumachowski, Weld J. 35 (1956) 521.
[5] J. Mittra, G.K. Dey, D. Sen, A.K. Patra, S. Mazumber, P.K. De, Scripta Mater. 51 (2004) 349.
[6] Z. Guo, W. Sha, D. Vaumousse, Acta Mater. 51 (2003) 101.
[7] J.W. Hooijmans, G.L. Tjoa, J.G. van der Laan, Material procurement and characterisation, TVV BOLMAT – Deliverable 1, NRG Report 20726/02.49439/I, 2002.
[8] F. Schmalz, J. Boskeljon, D.S. d'Hulst, P. ten Pierick, J. Rensman, J.G. van der Laan, Irradiation induced stress relaxation results for Alloy 625+ and PH13-8Mo, TW1-TVV Bolmat – Deliverable 3, NRG Report 20726/05.64920/P, 2005.
[9] W.E. Freudenreich, C.M. Sciolla, STROBO-03/04/05 (R350-03/04/05) Nuclear analysis, NRG Report K5079/02.47238/l, 2002.
[10] J.C.H. Spence, J.M. Zuo, Electron Microdiffraction, Plenum Press, New York, 1992.
[11] R.W.K. Honeycombe, Steels: Microstructure and Properties, Edward Arnold, London, 1981.
[12] L.S. Hung, M. Nastasi, J. Gyulai, J.W. Mayer, Appl. Phys. Lett. 42 (1983) 672.
[13] J. Weertman, J. Weertman, Elementary Dislocation Theory, The MacMillan Company, New York, 1964.
[14] M.L. Jenkins, M.A. Kirk, Characterization of Radiation Damage by Transmission Electron Microscopy, Institute of Physics Publishing, Bristol, 2001.
[15] A.L. Bement, Fundamental materials problems in nuclear reactors, in: Proceedings of the ICSMA 2 Conference, vol. 2, 1970, p. 693.
[16] R.E. Stoller, S.J. Zinkle, J. Nucl. Mater. 283–287 (2000) 349.
[17] N. Baluc, R. Schäublin, P. Spätig, M. Victoria, in: M.L. Grossbeck, T.R. Allen, R.G. Lott, A.S. Kumar (Eds.), Effects of Radiation on Materials: 21st International Symposium, ASTM STP, 1447, ASTM International, West Conshohocken, PA, 2003.